

Modeling and Diagnostic of an SF₆ RF Plasma at Low Pressure

C. Riccardi, *Member, IEEE*, R. Barni, F. De Colle, and M. Fontanesi

Abstract—This research concerns the experimental and theoretical analysis of an SF₆ radio-frequency (RF) discharge at low pressure in a small reactor for industrial applications. The plasma is produced in the pressure range of 0.05–1 mbar by a 13.56-MHz RF supplier at moderate power, up to 25 W. The pumping system sustains a flowrate of about 50 cm/s, with residence time in the discharge of about 0.2 s. The discharge parameters have been measured and lie in the range $n_e \cong 10^7$ – 10^9 cm⁻³, $n_i \cong 10^{10}$ – 10^{12} cm⁻³, $T_e \cong 5$ – 10 eV. Measurements were performed by means of movable electrostatic probes and of a phodiode. Particular care in the analysis of the data proved necessary due to the presence of a substantial amount of negative ions. On the other hand, we have performed simulations of the discharge composition through the implementation of a suitable numerical model of the chemical kinetics in the device. On the basis of the experiments a comparison of charge and neutral species production with those predicted by the theory was performed, and a more realistic description of the involved phenomena was obtained. In particular, several assumptions concerning the ion diffusion coefficient were tested, allowing us to pin down the relative importance of transport and bulk processes in the discharge state. PACS: 52.75.Rx, 52.25.Dg, 82.40.Ra.

Index Terms—Capacitively coupled discharges, chemical kinetics, diffusin and transport, modeling, plasma measurements, radio frequency plasma.

I. INTRODUCTION

THE RESEARCH on glow discharges is of great interest in industrial applications and in particular in the chemical vapor deposition (CVD) processes [1]. Depending on the gas mixture used for the plasma production, different processes like film deposition, etching, polymerization, and activation can be performed in order to modify the first surface layers of a material. The research in this field is mainly devoted to both the modeling of the plasma composition and the optimization of the processes [2]. This research concerns the experimental and theoretical analysis of an SF₆ radio-frequency (RF) plasma produced at low pressure (0.05–1 mbar) in a device for the activation and polymerization of materials, mainly, plastics and textile products [3].

The SF₆ plasma is quite a peculiar one: as a matter of fact, the large electronegativity of fluorine results in a large attachment cross section of electrons on radicals containing fluorine [4]. The ion composition is thus largely dominated by atomic and molecular negative ions with respect to electrons. Thus transport properties and the reactivity of such a plasma are very dif-

ferent from that of an ordinary noble gas one at the same external pressure and RF power [5]. The main aim of this work is the analysis of the chemical kinetics and of the transport of the activated species in a plasma reactor making a comparison between model predictions and experimental results. The analysis is performed checking the validity of the standard theoretical (numerical) models [6] used in the simulation of such systems by measuring the relevant plasma parameters and at the same time experimentally investigating the properties and the capabilities of such a plasma. The conditions determined by our setup are moderately high flow velocity (about 50 cm/s) and short residence times, of about 0.2 s. For this reason, the model should be formulated as a plug-flow reactor model [7] (in which the effect of the diffusion along the flow is not considered). In fact, in the pressure range of our experiments, the flow velocity exceeds the diffusion one, making the contribution of diffusion along the flow direction negligible. A more detailed description of such an approach can be found, for instance, in [8]. The model is able to predict the neutral and charged species densities as a function of several parameters, like neutral gas pressure, RF power, and position in the vacuum chamber. The experiments were performed in conditions similar to those assumed in the numerical code. On the basis of the experiments, a direct comparison of charged and neutral species production with that predicted by the theory can be performed. In particular, in order to obtain good agreement between experiments and theory, some unclear aspects had to be systematically discussed: the amount of negative ions, the particle transport, and the choice of the cross section data set. For what concerns the transport of charged particles, different models for particle diffusion [9] were considered and experimentally tested, and a quite exhaustive explanation of the more realistic assumptions for the transport was given. The amount of negative ions with respect to the electrons was analyzed varying the main plasma parameters like neutral density and RF power by means of Langmuir characteristic curves [10]. To this purpose, a discussion on the interpretation of Langmuir characteristics in the presence of negative ions based on theoretical assumptions [11], [12] and supported by experimental observations was done.

This paper is organized as follows: after a brief description of the apparatus, there is a discussion of the experimental techniques used in the characterization of the device, a presentation of the theoretical model employed for the simulation of the reactor performance, and a comparison of the numerical results with the collected data. In the end, we summarize the conclusions that can be derived from this work and some consideration on the goodness of the operative choices.

Manuscript received May 4, 1999; revised October 8, 1999.

The authors are with the Dipartimento di Fisica G. Occhialini, Università degli Studi di Milano-Bicocca e INFN, Milan 15 20126, Italy.

Publisher Item Identifier S 0093-3813(00)01703-3.

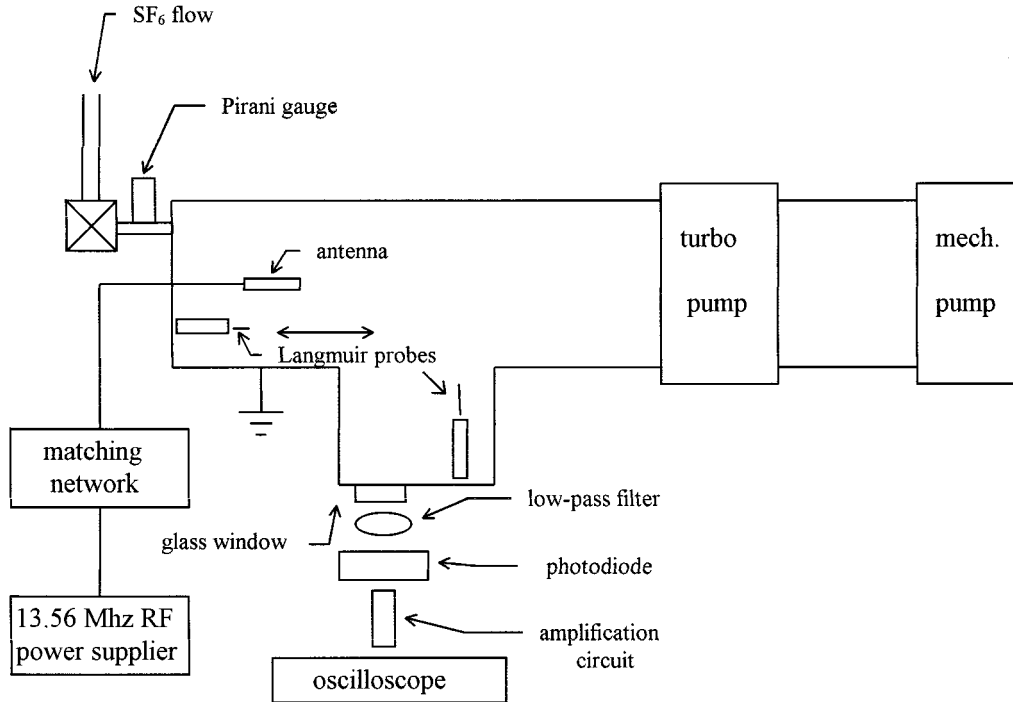


Fig. 1. Schematic view of the reactor setup.

II. EQUIPMENT SETUP

The reactor used for the experiments is sketched in Fig. 1. The vacuum chamber consists of a series of stainless-steel cylindrical tubes (10 cm diameter) with several ports for diagnostics. The chamber is evacuated by a pumping system composed of a turbo molecular pump and a rotary pump to a residual pressure of 10^{-6} mbar. The actual pressure in the reactor is determined by the position of a manual leakage valve connected to the SF₆ feeding system (at a pressure of 0.1 mbar, the flowrate Q is about 25 sccm). During operation, the pressure inside the chamber is monitored by a Pirani gauge (pressure P ranges between 10^{-2} and 1 mbar).

The plasma is generated by a capacitive antenna: a stainless-steel cylindrical pin (1 cm diameter, 2 cm length) axially located in the cylindrical vacuum chamber is fed with a RF voltage with respect to the same chamber, which is grounded. The antenna is then externally connected through a matching network to a 13.56-MHz RF power supplier (RFX600).

In such a configuration, the RF coupling is dominated by the large capacitance of the grounded reactor chamber [13]. The actual RF power in the reactor was measured by a wattmeter and ranges up to 25 W. The plasma generated in the reactor fills the vacuum chamber and extends longitudinally for about 10 cm around the antenna. The discharge parameters, measured as discussed below, are in the range $n_e \cong 10^7$ – 10^9 cm⁻³, $n_i \cong 10^{10}$ – 10^{12} cm⁻³, and $T_e \cong 5$ –10 eV.

III. EXPERIMENTAL DIAGNOSTICS OF THE REACTOR

In order to monitor the plasma parameters, movable electrostatic Langmuir probes have been used [10]. The measurements were taken with shielded Tungsten cylindrical probes (1 mm diameter and 5.8 mm length) insulated with a ceramic sleeve. The current characteristic of the probe is measured as a voltage drop

on a shunt resistance and read on a digital oscilloscope. The bias is swept in about 0.1 s, and for each sweep we collect 2000 data. The Langmuir probe was used without RF compensation [14]: in fact, for low operation power (less than 25 W), the RF distortion of the Langmuir characteristic can be considered negligible, as can be inferred from the measurements of floating potential at 13.56 MHz, which never exceed 80 mV and are much less than the static floating potential. The analysis of the Langmuir characteristic was performed in the framework of the orbited motion limited (OML) theory [15] in the case of a thin sheath, modified by the presence of negative ions in SF₆ plasma [11], [12]. By taking numerically the second derivative of the characteristic [16], it is possible to look also at the electron energy distribution function (EEDF) f_E , which appears indeed approximately Maxwellian and, therefore, can be completely parameterized by an electron temperature T_e . The positive ion density n_+ is extracted from the ion saturation current I_+ according to the formula of [11]

$$I_+ = q_+ \cdot S \cdot n_+ \sqrt{\frac{k_B \cdot T_-}{e \cdot M_+}} \quad (1)$$

where q_+ and M_+ are, respectively, the charge and mass of the ions (here supposed to be SF₅⁺, as suggested both by the simulation and by previous works on charged species mobility [17]), S is the probe collecting surface, and the square root represents the Bohm velocity of the ions entering the sheath. Here, T_- is the negative ion temperature, taken equal to the flowing gas one (0.025 eV). Such a formula, arising from the Bohm sheath criterion generalized for the presence of negative ions [11], is appropriate under the conditions $T_e \gg T_-$ and $n_+ \approx n_- > n_e$, which are met in most of the experiments in SF₆ plasma. When negative ions dominate, a presheath is created into which posi-

tive ions enter from the plasma bulk with a kinetic energy of the order of the thermal energy of the dominant negative charged specie ($k_B T_-$) [18]. Moreover, the approach of [11] was previously tested in the experiment of [19], which was performed in conditions very similar to ours, by independently measuring the positive and negative ion densities.

The electron temperature T_e is extracted from the slope of the linear fit of the logarithmic Langmuir characteristic along this formula

$$\log I(V) = \log I_0 - \frac{q_e}{k_B \cdot T_e} \cdot (V - V_{PI}) \quad (2)$$

where $I_0 = q_e \cdot S \cdot n_e \sqrt{(k_B \cdot T_e)/(2\pi \cdot m_e)}$ is the electron current at the plasma potential V_{PI} .

The plasma potential and thus the electron density are estimated from the Langmuir semilog plot by the intersection of the previous fit and the linear fit of the electron saturation region [16].

The discharge light emission was monitored by a photodiode (Centronics OSD357CQ), which operates from the near ultraviolet to infrared (200–1100 nm). The photodiode current signal is converted into a voltage output through a two-step amplification circuit based on an operational amplifier working in transimpedance mode. Typically 1-nA current, equivalent to a light intensity of about 2 nW, gives an output voltage of about 50 mV (after being filtered from the high-frequency external noise), which is measured on a digital oscilloscope. We have measured the photodiode circuit output observing the discharge with two different low bandpass filters ($\lambda \geq 600$ nm and $\lambda \geq 650$ nm) and without. By inserting a low bandpass filter ($\lambda \geq 650$ nm), we can measure the emission lines of fluorine radical (in fact electronic transitions from $2p^4 3p$ to $2p^4 3s$ levels give photons whose wavelengths lie between 600 and 800 nm; among these, the most prominent lines are the 685.6, 703.7, and 712.8 nm [20]). With such a cutoff wavelength, we are sure that a possible contamination from emission lines of SF_6 and other SF_x radicals is greatly reduced [21].

IV. NUMERICAL SIMULATION OF THE REACTOR

In a plasma reactor fed with an SF_6 gas, several different processes are at work, as summarized in the scheme of Fig. 2. The characteristic plasma chemistry processes are mainly driven by free electrons, which are by far the most energetic particles in the reactor, and include:

- 1) ionization reactions;
- 2) electronic transitions to excited energy levels responsible for the rich light emission spectra of the discharges, molecular excitations of reactive vibrational and rotational states;
- 3) molecular dissociation with production of highly reactive free radicals;
- 4) electron attachment, particularly important in highly electronegative gases such as the ones composed of fluorine, which is the main source of negative ions in the plasma.

The gas mixture composition in the reactor is determined by the chemical reactions between the reactive species and by the transport processes. The transport depends on the hydrodynam-

ical flow driven by the pumping system, by the diffusion of the neutral and charged species towards reactor walls, and by the surface interactions at gaseous–solid interface. The last process includes adsorption of gaseous species, which eventually react with the surface atoms, desorption of volatile species generated in the solid lattice, and sputtering due to energetic particles, mainly ions impinging onto the surface after being accelerated by the sheath at the walls.

A detailed simulation of the reactor performances requires the knowledge of several molecular mechanisms. Some of them are only poorly known, such as those crucially depending on the surface structure and composition (physical and chemical adsorption, sputtering yields). Moreover, the active processes are each characterized by its own times and magnitude, thus implying a considerable degree of complexity. Therefore, in order to keep the problem manageable, some approximations are needed.

As far as it concerns the plasma, we point out that the characteristic times ruling the discharge development are very short (RF cycle period $\tau_{RF} = 74$ ns, the confinement time for electrons drifting to the walls $\tau_d = 10$ μ s) compared to the ones governing the radical species transport and the gas-phase reactions: therefore the plasma produced in the reactor can be considered in a quasi-stationary state determined by the external working parameters (pressure P , flowrate Q , and RF power W_{RF}) and slowly adapting to the changes in the neutral species concentration. Therefore, the plasma evolution decouples almost completely from gas kinetics. The plasma-driven processes considered in the model can be fully characterized by prescribing the correct plasma state as an external condition, setting as parameters the electron density $n_e(r, z, t)$ and the EEDF $f_E(r, z, t)$. Despite the fact that several processes are involved in the electron energy losses, due to the rich molecular structure of the gas, the measured EEDF's appear in most of the cases approximately Maxwellian and, therefore, can be parameterized simply by an electron temperature $T_e(r, z, t)$.

The connection between such microscopic parameters and the external operative ones is assured by the analysis of the experimental Langmuir probe data. For instance, at fixed pressure, the electron density n_e comes out to be nearly proportional to the RF power feeding the discharge, while the electron temperature T_e is almost independent of it.

The problem of determining the evolution of the concentration of the different N species can be managed by writing the balance equation for each density $n_k(r, z, t)$ of the k th species

$$\frac{dn_k}{dt} = \Pi(k) - \Delta(k) \quad (3)$$

where d/dt is the total time derivative. The first term $\Pi(k)$ consists of the sum of all production processes of the k th species, due to both chemical reactions, in the gas phase or at the reactor surface, and to the external gas fed. It can be written as

$$\begin{aligned} \Pi(n_k) = & \sum_{i < j=1}^N K(i + j \rightarrow k) n_i n_j \\ & + \sum_{l=1}^N K(l \rightarrow l(w) \rightarrow k) n_l + Q(k(\text{in}) \rightarrow k) \end{aligned} \quad (4)$$

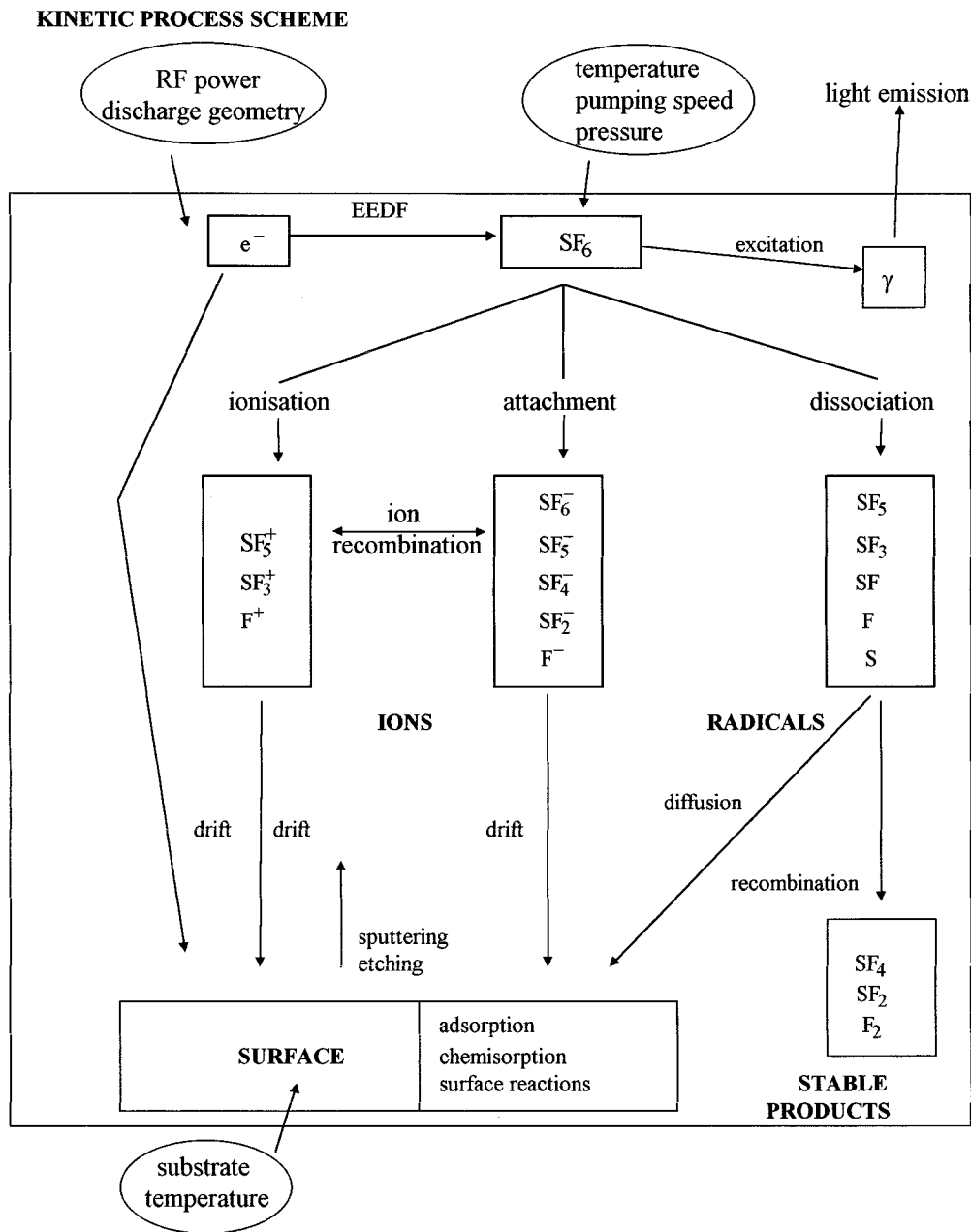


Fig. 2. Block diagram of the kinetic processes at work in an SF₆ plasma.

where K are the reaction rates for the gas phase reactions and the effective rate for the surface ones (consisting of the chain process: adsorption of species l , reaction at the surface and desorption of species k) and Q is the flowrate. In the same way, the contributions to the loss term Δ of the k th species are the destruction of k in a gas phase reaction, the diffusion followed by adsorption at the reactor surface and the pumping outside

$$\Delta(n_k) = \sum_{i,j=1}^N K(k+i \rightarrow j)n_k n_i + D(k \rightarrow k(w))\nabla^2 n_k + Q(k \rightarrow k(\text{out}))\frac{n_k}{n_{\text{tot}}} \quad (5)$$

where D is the diffusion coefficient of the k th species.

In parallel, a simulation of the hydrodynamical flow should also be performed, so that the right velocity field can be inserted in the total derivative in order to close the system of differential equations.

In a preliminary stage, some other simplification is worthy: since in normal operative conditions ($P = 0.1$ mbar, $Q = 25$ sccm), the Reynolds number is $\mathcal{R}e = 1.97$, a simple laminar flow in a cylindrical tube is an adequate representation of our reactor hydrodynamics. Moreover, since the flow velocity v_{flow} (at $P = 0.1$ mbar about 50 cm/s) exceeds the diffusion one ($V_{\text{diff}} = D/2R$ where R is the vacuum chamber radius and the so-called Peclet number $Pe = V_{\text{flow}}/V_{\text{diff}}$ is about 2) the effect of mixing in the flow direction can be safely ignored and a plug-flow approximation [7] is appropriate: this means that we

could neglect diffusion in the flow direction with respect to that in the radial one.

As a result, the geometry is slab and $(dn_k(r, z, t)/dt) \approx V \cdot (\partial n_k(r, z)/\partial z)$.

The equations can be further simplified treating the diffusion process according to [22], that is, approximating the transverse (radial) profile of the concentration as the first normal mode of the reactor chamber (in our cylindrical geometry the Bessel function $J_0(kr)$). Within this approximation, diffusion should be considered only for species that can be absorbed at the surface (for which the so-called sticking coefficient S is not zero) and its contribution to the loss term Δ becomes

$$D(k \rightarrow k(w)) \nabla^2 n_k(r, z) \approx \frac{D}{\Lambda^2} n_k(z) \quad (6)$$

where Λ^2 depends only on geometrical factors and on the sticking coefficient S [22].

So linearized, this differential equations system can be integrated by means of standard numerical techniques, for instance, using an adaptive Kutta-Runge routine such as DDEQMR¹. Additional time can be saved, especially in the early steps, by using as variables the logarithm of density and of time, thus effectively smoothing the system.

As a result, a complete mapping of the gas-phase composition and of the flows towards the surface is obtained. In order to reduce the species number N , we consider only the most important ion species according to the data of [23] and [24]. A more detailed simulation of the positively charged species composition requires knowledge, besides of the ionization processes, of the relevant charge exchange rates (usually quite fast), still lacking in literature. This explain why even if the main ionization reaction is by far the direct ionization of SF_6 to SF_6^+ , such an ion does not appear in the measured ion composition [17], [24]. All the species included in the simulation are shown in the scheme of Fig. 2.

The relevant reaction rates at the low-pressure conditions of the experiments were taken from the literature and are summarized in Table I. In particular for the ionization and dissociation rates we followed,² eventually integrating along the indications of [23] in the case of SF_x radicals and from [25] for multiple dissociation of SF_6 , whereas for electron attachment on SF_6 , we use the cross section fits of [26], extrapolated for radicals as in [23]. Recombination rates for ions were taken from [27] and for radicals from [23], [28]. Electron detachment was added for completeness, even if it comes out that it plays a minor role in negative ion kinetics. Diffusion coefficient for ions can be extracted from mobility studies [17], [26], while for fluorine and SF_x radical, we follow [26]. As far as concerns the sticking coefficients S , the value $S = 0$ was assumed for the stable species, while $S = 1$ is appropriate for charged particles. Unfortunately, the radical sticking coefficients are badly known. For instance, as regards the most interesting fluorine radical, $S \approx 1$ was used in the literature [23], [27], which fits for a continuously polished surface. However, we find it more appropriate to use a much lower value ($S \approx 0.007$, as was assumed in [28], on the basis of the measurements made on methane radicals in [29]) to describe the reactor walls in stationary condition

TABLE I
REACTION RATES CONSIDERED IN THE
NUMERICAL SIMULATION. THE RATES ARE CALCULATED FROM ARRHENIUS
TYPE FITS FOR AN ELECTRON TEMPERATURE $T_e = 7$ eV AND FOR A FLOWING
GAS PRESSURE $P = 0.1$ mbar AND TEMPERATURE $T = 293$ K

Nr.	Reaction	Rate (cm ³ /s)	References
1	$e^- + F_2 \rightarrow F + F + e^-$	0.35E-07	[2]
2	$e^- + SF_2 \rightarrow F + S + e^-$	0.19E-07	[23]
3	$e^- + SF_2 \rightarrow F + SF + e^-$	0.15E-07	[23]
4	$e^- + SF_3 \rightarrow F + SF_2 + e^-$	0.28E-07	[23]
5	$e^- + SF_4 \rightarrow F + SF_3 + e^-$	0.20E-07	[23]
6	$e^- + SF_5 \rightarrow F + SF_4 + e^-$	0.47E-07	[23]
7	$e^- + SF_6 \rightarrow F + SF_5 + e^-$	0.15E-07	[2]
8	$e^- + SF_6 \rightarrow F + F + SF_4 + e^-$	0.72E-09	[25]
9	$e^- + SF_6 \rightarrow F + F_2 + SF_3 + e^-$	0.21E-09	[25]
10	$e^- + SF_6 \rightarrow F + F + F_2 + SF_2 + e^-$	0.22E-09	[25]
dissociation			
11	$e^- + F \rightarrow F^+ + e^- + e^-$	0.10E-08	[2]
12	$e^- + F_2 \rightarrow F + F^+ + e^- + e^-$	0.14E-08	[2]
13	$e^- + SF_3 \rightarrow SF_3^+ + e^- + e^-$	0.12E-07	[23]
14	$e^- + SF_4 \rightarrow SF_4^+ + F + e^- + e^-$	0.13E-07	[23]
15	$e^- + SF_5 \rightarrow SF_5^+ + e^- + e^-$	0.13E-07	[23]
16	$e^- + SF_6 \rightarrow SF_6^+ + F + e^- + e^-$	0.52E-08	[2]
attachment and detachment			
17	$e^- + F \rightarrow F^-$	0.13E-09	[2]
18	$e^- + F_2 \rightarrow F + F^-$	0.18E-09	[30]
19	$e^- + SF_x \rightarrow SF_x^-$	0.31E-09	$x=1,6$ [23,26]
20	$e^- + SF_6 \rightarrow SF_5^- + F$	0.26E-09	[26]
21	$e^- + SF_6 \rightarrow SF_4^- + F_2$	0.13E-09	[26]
22	$e^- + SF_6 \rightarrow SF_4^- + F_2$	0.24E-11	[26]
23	$e^- + SF_5 \rightarrow SF_4^- + F$	0.81E-09	[23,26]
24	$e^- + SF_5 \rightarrow SF_4^- + F$	0.41E-09	[23,26]
25	$e^- + SF_4 \rightarrow SF_3^- + F$	0.34E-09	[23,26]
26	$e^- + X^- \rightarrow X + e^- + e^-$	0.34E-08	[27,30]
ion recombination			
27	$X^+ + Y^- \rightarrow X + Y$	0.10E-07	[27]
neutral recombination			
28	$F_2 + SF_x \rightarrow F + SF_{x+1}$	0.70E-14	$x=0,5$ [23]
29	$F + SF_x \rightarrow SF_{x+1}$	0.25E-12	$x=0,5$ [23]
30	$F + F \rightarrow F_2$	0.51E-18	[30]
31	$SF + SF \rightarrow S + SF_2$	0.18E-10	[28]
32	$SF + SF_2 \rightarrow S + SF_3$	0.13E-10	[28]
33	$SF + SF_3 \rightarrow SF_2 + SF_4$	0.11E-9	[28]
34	$SF_3 + SF_3 \rightarrow SF_2 + SF_4$	0.22E-11	[28]
35	$SF_3 + SF_3 \rightarrow SF_2 + SF_4$	0.40E-11	[28]
36	$SF_3 + SF_3 \rightarrow SF_4 + SF_6$	0.95E-12	[28]

of operation, when an adsorbed fluorine monolayer has covered the vacuum chamber walls [30].

V. RESULTS

The evidence of negative ions comes directly by measuring Langmuir characteristics. A typical radial profile obtained by means of the Langmuir diagnostic technique is shown in Fig. 3. Considering as the majority positive ion species the SF_5^+ , the electron $\{o\}$ and the positive ion $\{\bullet\}$ densities derived by Langmuir curves for the typical discharge parameters are, respectively, $5 \cdot 10^7$ cm⁻³ and $5 \cdot 10^{10}$ cm⁻³. While the electron temperature profile $\{\Delta\}$ is rather flat, density profiles of electrons and ions are similar and approximately parabolic.

¹CERNLIB is the C.E.R.N. Program Library: <http://wwwinfo.cern.ch/asd/>.

²KINEMA database: <http://www.csn.net/~morgan/database.htm>.

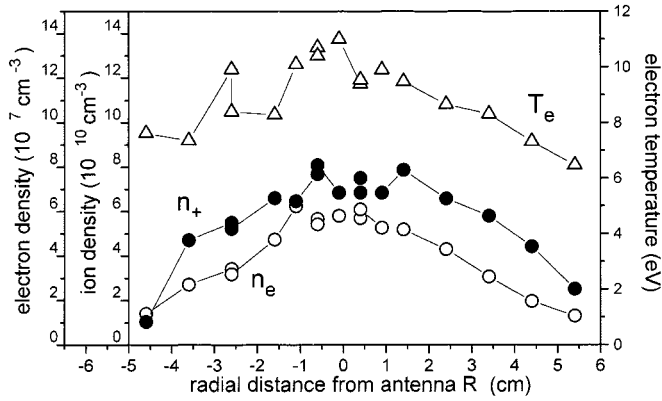


Fig. 3. Radial profile of positive ion {•} and electron {○} density and of electron temperature {△} at the working conditions of $W_{RF} = 10$ W, $P = 0.1$ mbar, and longitudinal distance from antenna $Z = 3.5$ cm).

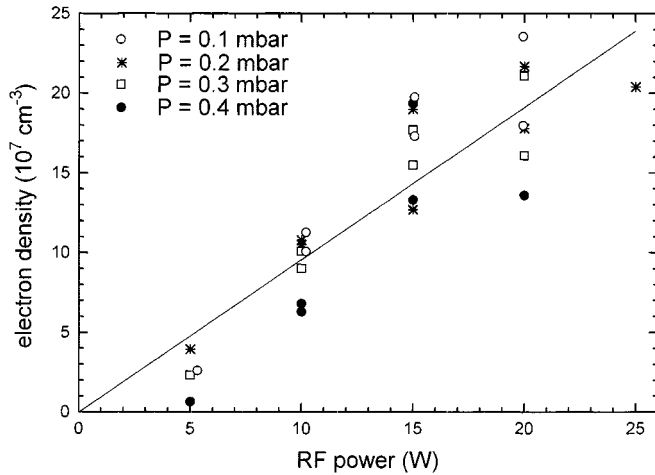


Fig. 4. Electron density as a function of the delivered RF power at different pressures ($P = 0.1$ {○}, 0.2 {*}, 0.3 {□}, 0.4 {•} mbar). The straight line just underlines the proportionality between the two quantities.

Varying the RF power between 2 and 25 W and the neutral gas pressure from 0.05 to 0.5 mbar, the ion to electron density ratio η ranges between 1000 and 5000, suggesting the dominance of negative ions in the SF₆ plasma. The expected composition of the negative ion population can be established considering the kinetics of electron attachment process: SF₆⁻ and SF₅⁻ are produced by low energy electron impact on SF₆, while the threshold for F⁻ formation is around 4 eV. Thus, the latter can dominate only at a rather large electron temperature [31]. Electron density comes out to be nearly independent of pressure and almost proportional to the delivered RF power, as it can be appreciated from Fig. 4. Electron temperature and density, derived from the analysis of the Langmuir probe data, can be used as input parameters of the numerical simulations, thus allowing a comparison between the values of the ratio η experimentally found and the predicted ones. One can therefore check whether the simulation of the plasma composition is fairly correct.

In order to numerically derive the plasma and neutral gas mixture composition, some basic considerations on the transport processes, supported by experimental results, have to be made. The transport properties of such a plasma are completely different from electrons dominated plasmas. Particular care is to

be paid in the treatment of ion diffusion. In most discharges, the large electron mobility induces an ambipolar electric field modifying positive and negative ions drift velocities, but this is not the SF₆ case. The first consideration is that the presence of a large amount of negative ions invalidates the standard ambipolar diffusion formula ($D_{amb} = D_{free} \cdot (1 + T_e/T_{\pm})$) used for instance in [23]. On the other hand, considering only free ion diffusion losses, as in [27], an unphysical violation of quasi-neutrality in the bulk plasma occurs because of the different diffusion velocities of electrons and ions. In our simulations, we chose the approach of Lichtemberg *et al.* [32], where the charge balance equations have been considered.

Since in numerical simulations the electron density is fixed and equal to the electron density determined from experimental data, neglecting the very small electron recombination rate, the electron diffusion losses are determined by balancing electron production, namely, ionization, with attachment process. Then charge balance equations imposing quasi-neutrality fix the local electric field and the diffusion loss term for positive ions.

As far as regards negative ions, we consider only free diffusion followed by detachment in the wall sheaths [23]. At variance with [32], we do not impose a null negative ion flux: in fact, a consequence of the absence of negative ion diffusion is the prediction of a flat electron radial profile ($\nabla n_e/n_e \ll \nabla n_i/n_i$), which is ruled out by our experimental data, as can be seen, for instance, in Fig. 3.

Different hypotheses regarding the effective ion diffusion coefficients lead to quite different predictions of the η values, as shown in Fig. 5, reporting η for experimental data and different simulation implementation of the transport processes.

A numerical simulation considering an ambipolar diffusion {□} results in η values of about 100, an order of magnitude smaller than the observed ones {•}, and therefore can be excluded in the reactor conditions. On the other hand, the simulation involving balanced ion diffusion (Lichtenberg [32]) {○} and {△} are given by simulations obtained for two choices of the ion recombination rates (K_{rec}) performs very well in all the experimental conditions varying both pressure and RF power. Since the effective ion drift velocity is rather small (about 15 cm/s for SF₅⁺), typical of an almost free diffusion mechanism, in our reactor geometry the η value is determined by the bulk recombination rate. Therefore, some sensitivity can be claimed also about the magnitude of this parameter, although the effect is not so striking. The comparison with the experimental data points out that a better agreement can be achieved using the rather low rates ({○} in Fig. 5, with $K_{rec} \approx 10^{-8}$ cm³/s) taken from [26] and not the ten times larger ones ({△} in Fig. 5, with $K_{rec} \approx 10^{-7}$ cm³/s), extrapolated from atomic recombination (H⁺H⁻, O⁺O⁻) used in the simulation of [27]. In fact, the simulation carried out with the larger rates produces η values systematically lower than experimental values.

In spite of the rather crude approximation made in [32], namely, that of a flat electron density radial profile, such a model is nevertheless able to reproduce the correct behaviour of η with the simple formula (represented by {*} in Fig. 5)

$$\eta = \sqrt{\frac{15}{8} \cdot \frac{K_{att} \cdot n_{SF_6}}{K_{rec} \cdot n_e}}. \quad (7)$$

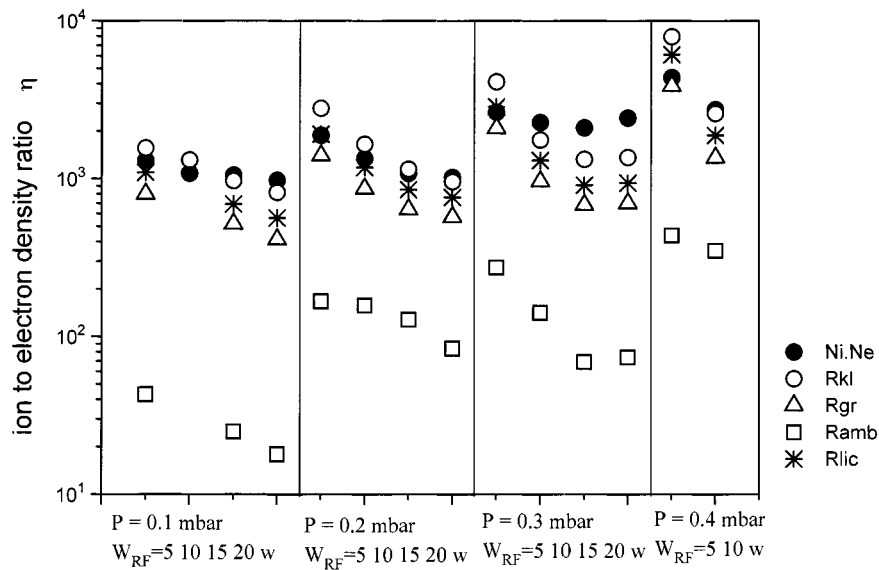


Fig. 5. Behavior of ion to electron density ratio η in the range of pressure and RF power studied in the experiments. Different simulation parameters are compared with the data. $\{\bullet\}$ = experimental results; $\{\square\}$ = ambipolar diffusion, $\{\circ\}$ = balanced free diffusion with the ion recombination rate, $K_{\text{rec}} \approx 10^{-8} \text{ cm}^3/\text{s}$, $\{\Delta\}$ = the same but with the higher ion recombination rate $K_{\text{rec}} \approx 10^{-7} \text{ cm}^3/\text{s}$, $\{*\}$ = (7) formula [32].

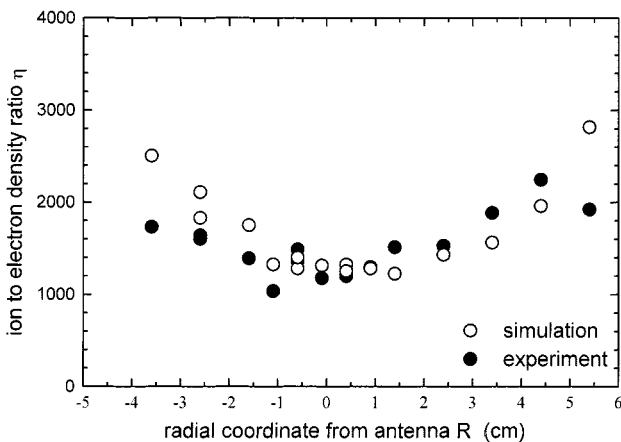


Fig. 6. Comparison between the ion to electron density ratio η extracted from the experimental radial profile shown in Fig. 3 ($W_{\text{RF}} = 10 \text{ W}$, $P = 0.1 \text{ mbar}$) $\{\bullet\}$ and the one predicted from the simulation $\{\circ\}$.

This formula reproduces the correct dependence between η and P and between η and W_{RF} . In fact, the experimental results show a slow increase of η with P (to be compared with the behavior $\eta \propto \sqrt{n_{\text{SF}_6}} \propto \sqrt{P}$ of (7)) and a decrease of η with W_{RF} , which at low power is proportional to the electron density n_e , reproduced by the dependence $\eta \propto \sqrt{1/n_e}$ of (7).

The comparison between the experimental and theoretical η values of radial profile is quite good, as shown in Fig. 6. The increase of η values near the vacuum chamber edge ($R = -5$) can be interpreted using (7), as due to the reduction of the electron density at the edges and, to a lesser extent, to the slight decrease of the electron temperature resulting in a greater attachment rate. The overall agreement between the simulation and the data on the η value in accessible electron density and temperature ranges is sketched in Figs. 7 and 8. In particular, the steep rise of η at low electron density is correctly reproduced by the simulation at different external pressures, while the difficulty in obtaining

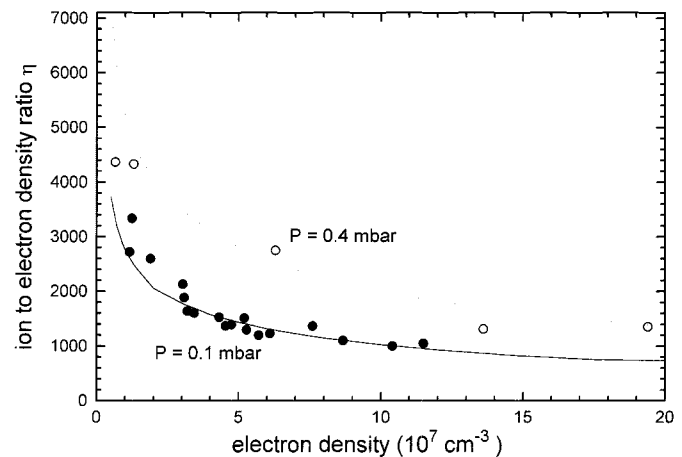


Fig. 7. Comparison between the positive ion to electron density ratio η extracted from the experimental data ($T_e \approx 8\text{--}10 \text{ eV}$, $P = 0.1 \{\bullet\}$, $0.4 \{\circ\}$ mbar) and the one predicted from the simulation at the same pressures with a fixed electron temperature $T_e = 9 \text{ eV}$ (full and dashed lines, respectively).

a wide electron temperature range keeping a constant electron density prevents a sharper test of the behavior predicted by the simulation and displayed in Fig. 8.

An example of the evolution of the neutral and ion species concentrations as predicted by the model is shown in Fig. 9. The simulation shows that total dissociation is rather small and only partially developed, with dominant radicals F, SF_4 , and SF_5 , while SF_2 and F_2 are somewhat less abundant. The important fluorine radical reaches equilibrium quite fast and is quickly diffusing and recombined onto the walls downstream. The neutral gas composition stays rather constant inside the plasma, with stable specie density slowly increasing along the flow direction. A large dissociation cannot be achieved in the reactor with such flowrates and such rather low powers. On the other hand, plasma composition reaches almost instantaneously a stationary condition far in advance the neutral gas phase.

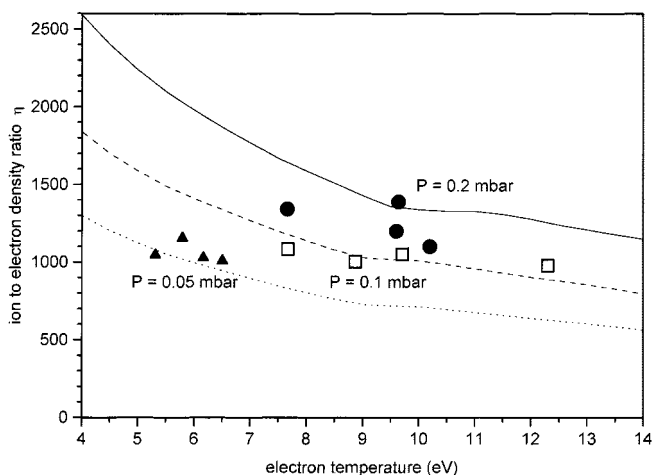


Fig. 8. Comparison between the ion to electron density ratio η extracted from the experimental data ($n_e \cong 1\text{--}1.2 \cdot 10^8 \text{ cm}^{-3}$, $P = 0.05$ $\{\Delta\}$, 0.1 $\{\square\}$, 0.2 $\{\bullet\}$ mbar) and the one predicted from the simulation at a fixed electron density $n_e = 1.1 \cdot 10^8 \text{ cm}^{-3}$ (dotted, dashed, and full lines, respectively).

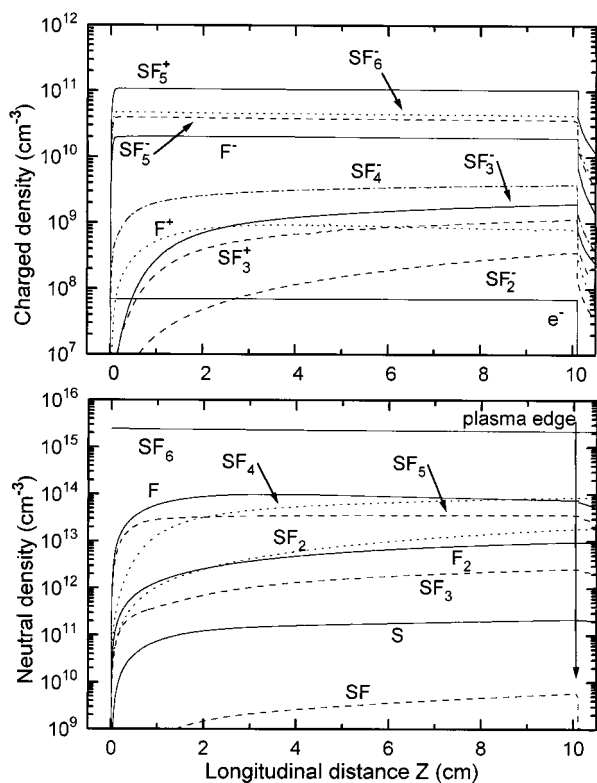


Fig. 9. An example of the variation along the axis of the vacuum chamber of the neutral and charged species densities as predicted by the simulation ($n_e = 7 \cdot 10^7 \text{ cm}^{-3}$, $T_e = 7 \text{ eV}$, $P = 0.1 \text{ mbar}$).

Due to the low dissociation level, the dominant positive ion is SF_3^+ deriving from ionization of SF_6 , with SF_3^+ ion becoming important only at substantial dissociation and relatively downstream, while F^+ ion is always a minority component in the conditions of our experiments. This result justifies the choice of the SF_3^+ mass as the effective positive ion mass made in the analysis of Langmuir characteristics. An interesting question is whether

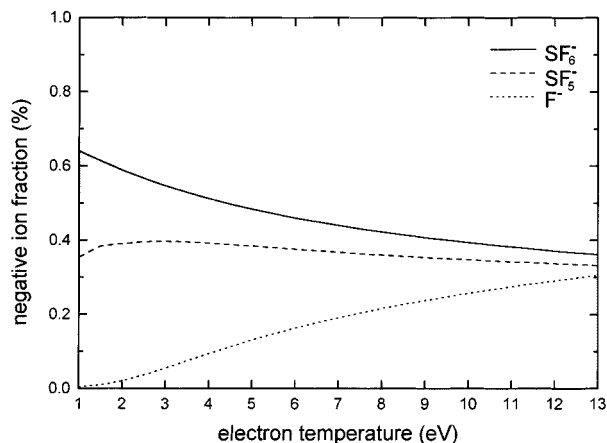


Fig. 10. The percentage of the different negative ion species with respect to the total negative ion density as a function of the electron temperature predicted by the simulation (SF_6^- is the full line, SF_5^- dotted, and F^- dashed).

the highly dissociated radicals arise from a chain of single dissociation reactions or directly from SF_6 through a multiple dissociation process. By suppressing the relevant rates in the simulation, it can be shown that SF_4 density is not affected by the dissociation channel considered (varying from 8.6 to $9.5 \cdot 10^{13} \text{ cm}^{-3}$ in simulations including only single or multiple dissociation channel or both) and that about 70% of SF_2 density is due to direct dissociation of SF_6 . However, it should be kept in mind that many of the relevant rates were never directly measured but only estimated, as, for example, the quoted branching ratio of SF_6 to SF_2 dissociation [25]. So these figures are somewhat uncertain, and existing simulations [23], [29], including only the chain of single dissociation reactions, should be adequately realistic. The negative ion component is built up of SF_6^- , SF_5^- , and F^- . The last one is produced mainly in dissociative attachment on SF_6 [4], [33], and its fraction increases with the electron temperature, as can be appreciated by the simulation results shown in Fig. 10. Again, a careful inspection of the simulation shows that less than 10% of F^- density arises from direct attachment on fluorine or from other radicals.

In view of the possible applications of our reactor for surface treatments, one of the most important parameters is the fluorine radical concentration, which depends on the balance between production by electron impact dissociation and recombination and diffusion losses. In order to gain insight into such parameters in different operation conditions, we have observed the discharge with a photodiode coupled with suitable filters. By taking the difference between the photodiode output with and without the 600-nm filter, we can select the short wavelength part of the spectrum (in the range from 200 to 600 nm), which is nearly proportional to the electron density, as extracted from the Langmuir probe analysis. The purely linear dependence on electron density disfavors fluorine and other radicals and therefore points towards a continuum contribution, also, if we cannot exclude emission line from SF_6 . Therefore, each emission light can be possibly ascribed to plasma bremsstrahlung radiation as, for instance, was observed in the experiments mentioned in [23].

The photodiode output current collected with the two low-pass filters comes from light emission in the red spectral region, mainly from deexcitation of excited fluorine energy

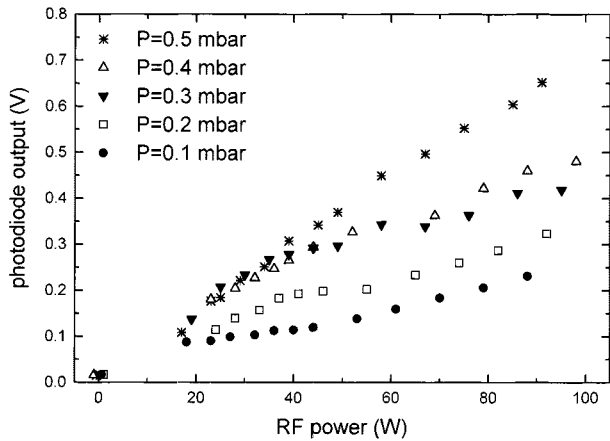


Fig. 11. Photodiode circuit output voltage as a function of the delivered RF power at different pressures between 0.1 and 0.5 mbar ($P = 0.1$ {●}, 0.2 {□}, 0.3 {▼}, 0.4 {△}, 0.5 {*}). The discharge was observed through the 600 nm low-pass filter.

levels [21], which in turn get populated by electron impact reactions. Two different channels are to be considered: in the first one, dissociation of SF_6 molecules can lead to excited fluorine radicals through the process $e^- + \text{SF}_6 \rightarrow e^- + \text{SF}_5 + \text{F}^*$, while in the second free fluorine, radicals in the ground state are excited by inelastic electron collisions through the process $e^- + \text{F} \rightarrow e^- + \text{F}^*$. The second mechanism is considered to be the dominant one in typical discharge conditions [21].

The small difference (less than 5%) between the data taken with the two filters shows also that the contribution of the continuum is negligible and cannot affect our measurements in the wavelength range $\lambda > 650$ nm.

Typical photodiode output data are shown in Fig. 11. A systematic trend towards larger photodiode outputs is observed when both pressure (and with it the total number density) and RF power (roughly proportional to the electron density n_e as experimentally checked by the Langmuir data analysis at least at low RF power; see Fig. 4) are increased. The numerical simulation shows that indeed the fluorine radical density displays a similar behaviour, as can be appreciated comparing the experimental data of Fig. 11 with the theoretical results of Fig. 12.

VI. CONCLUSION

We have presented a detailed analysis of the characteristics of an SF_6 plasma reactor. The peculiarities of such a chemical compound show up in the particular kind of plasma produced in the discharge (almost an electronless one) and in the transport properties of such a system. Nevertheless, a clarification of the relevant mechanisms determining the steady state reached in the device can be obtained with the joint effort of a suitable experimental diagnostic and of a detailed numerical simulation of the chemical kinetics. In particular, we want to stress the following points.

- 1) Plasma equilibrium composition in our (rather typical) vacuum chamber geometry can be described by the recombination process in the hypothesis of balanced ion

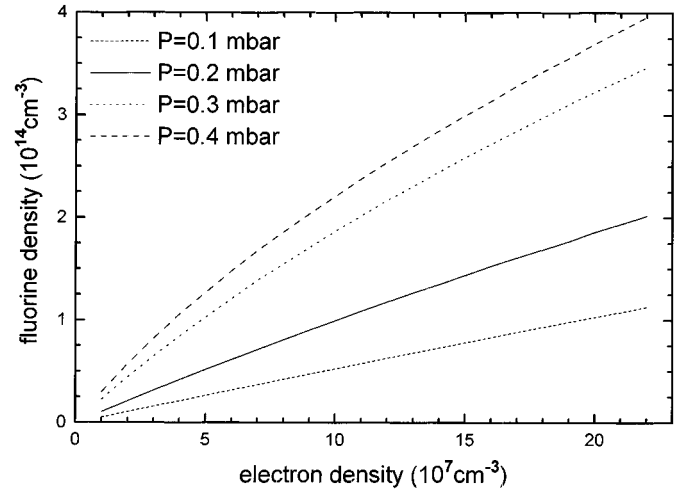


Fig. 12. Fluorine radical density as a function of the electron density at a fixed electron temperature $T_e = 9$ eV and at different pressures ($P = 0.1$ mbar is the short dashed line, 0.2 solid, 0.3 dotted, and 0.4 dashed).

diffusion [32]. This fact can be exploited both in pinning down the relevant reaction rates (at least at the right order of magnitude level) and in the search of the optimum operation conditions.

- 2) The ion to electron density ratio η in the plasma has demonstrated to be a sensible indicator also of the actual ion diffusion and of the other loss processes. We can conclude that a realistic description of these processes in such a plasma requires the full implementation of the charge balance equations and cannot be achieved with simpler approximations such as a standard ambipolar diffusion formula or a free (that is, at the same velocity of the neutral species) diffusion.
- 3) The practice of a Langmuir probe diagnostic technique proves very useful in the characterization of the plasma state produced in the device, all the more in view of the cheapness and the simplicity of the implementation of such an experimental method. In particular, it is able to measure the η values, which are relevant in the understanding of the plasma transport processes.
- 4) The concentration of free radicals, as, for instance, fluorine, which are relevant for the surface treatments, can be determined by the numerical simulation and the results agree with the experimental optical observations.
- 5) A numerical simulation of the chemical kinetic of such systems can be quite easily accomplished, but in order to obtain fully realistic predictions of the reactor performances, it should be carefully tested with the experimental observations. Then, after such an "optimization" procedure, the simulation can become a very useful tool in the analysis of the capabilities of the device in order to study the applications to surface treatments.

ACKNOWLEDGMENT

The authors would like to thank L. Gamberale for help in the development of the numerical code and M. Piselli for technical support.

REFERENCES

- [1] O. Auciello, A. Gras-Marti, J. A. Valles-Abarca, and D. L. Flamm, Eds., *Plasma Surface Interactions and Processing of Materials*. Dordrecht, the Netherlands: Kluwer Academic, 1990. C. Weissmantel, "Ion-based growth of special films: Techniques and mechanisms," *Thin Solid Films*, vol. 92, pp. 55–63, 1982.
- [2] L. Polak and Y. A. Lebedev, Eds., *Plasma Chemistry*. Cambridge, UK: Cambridge International Science. *Principles of Plasma Discharges and Materials Processing*, M. A. Lieberman and A. J. Lichtenberg, Eds. New York: Wiley, 1994.
- [3] S. Han, Y. Itoh, C. Sheen, and T. Tsui, "Polymer surface modification by plasma source ion implantation," *Surface Coatings Technol.*, vol. 93, pp. 261–264, 1997. N. V. Bhat and Y. N. Benjamin, "Surface Resistivity of Plasma Treated and Plasma Grafted Cotton and Polyester Fabrics," *Textile Res. J.*, vol. 69, pp. 38–42, 1999.
- [4] M. Hayashi and T. Nimura, "Importance of attachment cross sections of F⁻ formation for the effective ionization coefficients in SF₆," *J. Phys. D*, vol. 17, pp. 2215–2223, 1984.
- [5] E. W. McDaniel, *Atomic Collisions*. New York: Wiley, 1993.
- [6] M. J. Kushner, "A kinetic study of the plasma-etching process," *J. Appl. Phys.*, vol. 53, pp. 2923–2938, 1982. G. R. Misium, A. J. Lichtenberg, and M. A. Lieberman, "Macroscopic modeling of radio-frequency plasma discharges," *J. Vac. Sci. Technol.*, vol. A7, pp. 1107–1012, 1989.
- [7] J. M. Smith, *Introduction to Chemical Engineering Thermodynamics*. New York: McGraw-Hill, 1987.
- [8] A. Rhallabi and Y. Catherine, "Computer simulation of a carbon deposition plasma in CH₄," *IEEE Trans. Plasma Sci.*, vol. 19, pp. 270–277, 1991.
- [9] C. H. Mueller and A. V. Phelps, "Low current electric discharges in H₂/He mixtures," *J. Appl. Phys.*, vol. 51, pp. 6141–6148, 1980.
- [10] I. H. Hutchinson, *Principles of Plasma Diagnostics*. Cambridge, U.K.: Cambridge Univ. Press, 1987.
- [11] H. Amemiya, B. M. Annaratone, and J. E. Allen, "The collection of positive ions by spherical and cylindrical probes in an electronegative plasma," *Plasma Sources Sci. Technol.*, vol. 8, pp. 179–190, 1999. J. E. Allen, "Probe theories and applications: Modern aspects," *Plasma Sources Sci. Technology*, vol. 4, pp. 234–240, 1995; N. St. J. Braithwaite and J. E. Allen, "Boundaries and probes in electronegative plasmas," *J. Phys. D*, vol. 21, pp. 1733–1737, 1988.
- [12] H. Amemiya, "Plasmas with negative ions: Probe measurements and charge equilibrium," *J. Phys. D*, vol. 23, pp. 999–1013, 1990.
- [13] Y. Catherine and P. Coudrec, "Electrical characteristics and growth kinetics in discharges used for plasma deposition of amorphous carbon," *Thin Solid Films*, vol. 144, pp. 265–280, 1986.
- [14] U. Flender, B. H. Nguyen Thai, K. Wiesemann, N. A. Khoromov, and N. B. Kolokolov, "RF harmonic suppression in langmuir probe measurements in RF discharges," *Plasma Sources Sci. Technol.*, vol. 5, pp. 61–69, 1996.
- [15] L. Schott, *Plasma Diagnostics*, W. Lochte-Holtgreven, Ed. Amsterdam, the Netherlands: North-Holland. J. G. Laframboise, "Theory of spherical and cylindrical Langmuir probes in a collisionless Maxwellian plasma at rest," Ph.D. dissertation, Inst. Aerospace Studies, Toronto University, Canada, 1966.
- [16] V. A. Godyak, *Plasma Surface Interactions and Processing of Materials*, O. Auciello, A. Gras-Marti, J. A. Valles-Abarca, and D. L. Flamm, Eds. Dordrecht, the Netherlands: Kluwer Academic, 1990.
- [17] K. P. Brand and H. Jungblut, "The interaction potentials of SF₆ ions in SF₆ parent gas determined from mobility data," *J. Chem. Phys.*, vol. 78, pp. 1999–2012, 1983. F. L. Aravena and M. Saporoschenko, "Mobilities of positive ions in SF₆ gas," *J. Chem. Phys.*, vol. 98, pp. 8888–8891, 1993.
- [18] S. K. Kanakasabapathy and L. J. Overzet, "A coupled two-sheath simulation of RF bias at high electronegativities," *Plasma Sources Sci. Technol.*, vol. 7, pp. 289–297, 1998.
- [19] E. Stamate and K. Ohe, "Determination of negative ion and electron parameters in an Ar/SF₆ plasma," *J. Appl. Phys.*, vol. 84, pp. 2450–2458, 1998.
- [20] A. R. Striganov and N. S. Sventitskii, *Tables of Spectral Lines of neutral and Ionized Atoms*. New York: Plenum, 1968.
- [21] M. J. Kushner, H. M. Anderson, and P. J. Hargis, *Plasma Synthesis and Etching of Electronic Materials*, P. H. Chang and B. Abeles, Eds. New York: Elsevier, 1985.
- [22] P. J. Chantry, "A simple formula for diffusion calculations involving wall reflection and low density," *J. Appl. Phys.*, vol. 62, pp. 1141–1148, 1987.
- [23] H. M. Anderson, J. A. Merson, and R. W. Light, "A kinetic model for Plasma Etching in a SF₆/O₂ RF discharge," *IEEE Trans. Plasma Sci.*, vol. PS-14, pp. 156–164, 1986.
- [24] J. J. Wagner and W. W. Brandt, "DC plasma etching of silicon by SF₆, mass spectroscopic study of the discharge products," *Plasma Chem. Plasma Proc.*, vol. 1, pp. 201–215, 1981.
- [25] R. J. Van Brunt and J. T. Herron, "Plasma chemical model for decomposition of SF₆ in a negative glow corona discharge," *Physica Scripta*, vol. T53, pp. 9–29, 1994.
- [26] J. P. Novak and M. F. Fréchette, "Transport Coefficients of SF₆ and SF₆-N₂ mixtures from revised data," *J. Appl. Phys.*, vol. 55, pp. 107–119, 1984.
- [27] I. S. Grigoriev and E. Z. Meilikhov, Eds., *Handbook of Physical Quantities*. Boca Raton, FL: CRC Press, 1997.
- [28] J. B. Belhaouari, J. S. Gonzales, and A. Gleizes, "Simulation of a decaying SF₆ arc plasma: hydrodynamics and kinetics coupling study," *J. Phys. D*, vol. 31, pp. 1219–1231, 1998.
- [29] L. E. Kline, "Electron and chemical kinetics in the low-pressure RF discharge etching of silicon in SF₆," *IEEE Trans. Plasma Sci.*, vol. 14, pp. 145–156, 1986.
- [30] D. Edelson and D. L. Flamm, "Computer simulation of a CF₄ plasma etching silicon," *J. Appl. Phys.*, vol. 56, pp. 1522–1531, 1984.
- [31] H. Kojima, H. Sugai, and H. Toyoda, "Observation of CH₂ radical and comparison with CH₃ radical in a RF methane discharge," *Appl. Phys. Lett.*, vol. 13, pp. 1292–1294, 1989.
- [32] S. J. MacGregor, G. A. Woolsey, D. B. Ogle, and O. Farish, "The influence of electrode-fluorine reactions on corona and glow discharges in SF₆," *IEEE Trans. Plasma Sci.*, vol. PS-14, pp. 538–543, 1986.
- [33] L. E. Kline, D. K. Davies, C. L. Chen, and P. J. Chantry, "Dielectric properties for SF₆ and SF₆ mixtures predicted from basic data," *J. Appl. Phys.*, vol. 50, pp. 6789–6796, 1979.
- [34] A. J. Lichtenberg, I. G. Kouznetsov, Y. T. Lee, M. A. Lieberman, I. D. Kaganovich, and L. D. Tsendin, "Modeling plasma discharges at high electronegativity," *Plasma Sources Sci. Technol.*, vol. 6, pp. 437–449, 1997.



C. Riccardi (M'94) was born in Milan, Italy, on May 23, 1963. She received the Ph.D. degree in physics from the University of Milan in 1993.

Since 1993, she has been with the University of Milan in the Plasma Physics Laboratory, working on experimental plasma physics research: plasma turbulence, plasma-wave interactions, and plasma sources and diagnostics.



R. Barni was born in Pavia, Italy, on August 19, 1965. He received the Ph.D. degree in physics from the University of Milan, Milan, Italy, in 1993.

His present research interests concern surface treatments of materials and the chemical and plasma kinetics from both a theoretical and an experimental point of view.

F. De Colle was born in Como, Italy, in 1973. He works at the Plasma Laboratory of the University of Milan, Milan, Italy, on the implementation and exploitation of plasma diagnostics for industrial application devices.

M. Fontanesi was born in Rome, Italy, in 1939. He received the physics degree. Since 1977, he has been a Full Professor of General Physics at the University of Milan, Italy.

Together with P. Caldirola and E. Sindoni, he started the research activity in plasma physics in Milan. Recently, he has worked on the stationary toroidal plasma device Thorello studying plasma-wave interactions. He is also engaged in industrial applications of plasmas.